Surface-induced nematic and smectic order at a liquid-crystal–silanated-glass interface observed by atomic force spectroscopy and Brewster angle ellipsometry

K. Kočevar
J. Stefan Institute, Jamova 39, 1000 Ljubljana, Slovenia

I. Muševič*
Faculty of Mathematics and Physics, University of Ljubljana, Jadranska 19, 1000 Ljubljana, Slovenia
and J. Stefan Institute, Jamova 39, 1000 Ljubljana, Slovenia
(Received 13 April 2001; published 16 January 2002)

We have investigated nematic and smectic surface-induced ordering in the isotropic phase of the 4-cyano-4′-*n*-octylbiphenyl liquid crystal on silanated BK7 and LaSF glass using atomic force spectroscopy and Brewster angle ellipsometry. We have observed complete wetting of the silanated glass surfaces with the nematic phase when approaching the isotropic-nematic phase transition from above. Using the atomic force spectroscopy at the same interfaces, we have detected a significant presmectic ordering that is enhanced at the nematic-isotropic transition. We have observed the first, strongly adsorbed layer of liquid-crystalline molecules underneath this presmectic ordering. This first molecular layer is laterally inhomogeneous with typically 100 nm voids and covers approximately 70% of the surface. It is stable far above the clearing point and is responsible for the surface-memory effect. The results have been analyzed using Landau–de Gennes theory. The surface coupling energies of the nematic and smectic order have been determined, as well as the coupling energy between the nematic and smectic order.

DOI: 10.1103/PhysRevE.65.021703 PACS number(s): 61.30.Hn, 68.08.−p, 61.30.Eb

I. INTRODUCTION

It is well known that the breaking of the continuous translational and orientational symmetry of a liquid by a flat surface induces stratification and oscillations in the density and orientational order of the liquid at the liquid-solid interface [1]. This phenomenon is especially interesting in liquid crystals, because the surface-induced order can propagate into the bulk liquid crystal over mesoscopic or even macroscopic distances. In many cases it is relatively easily observable because of the strong optical and structural anisotropy of liquid crystals. This makes solid-liquid-crystal interfaces interesting from the fundamental aspects of many surface-related phenomena like surface wetting, dewetting, etc. It is of course of a fundamental technological importance, because the operation of liquid-crystalline devices is based on surface-induced alignment. The understanding of the physics and chemistry of these interfaces is therefore of prime technological importance.

Surfaces may induce significant surface orientational order even in the bulk isotropic phase of nematic liquid crystals, as first shown by Sheng and Miyano [2,3]. The surface-induced order is most significant very close to the phase transition into the nematic phase, where the system is soft and susceptible to external fields. The behavior of surface-induced order in this temperature region may give a detailed insight into the nature of surface-liquid-crystal coupling. This is the reason why the pretransitional surface-induced orientational order has been studied by a number of authors using different experimental methods, such as, for example, optical birefringence [2,3], ellipsometry [4–6], second-harmonic generation [7], nuclear-magnetic-resonance [8–10], x rays [11], and specific heat [12]. These methods are macroscopic and are measuring only an average orientational or positional order of the liquid crystal across the interface. Some of these methods observe the structure of the interface in a reciprocal space and all of them demand fitting of the spectra to the model interfaces. Direct space observation of the solid-liquid-crystal interface were reported using scanning tunneling microscope [13] and surface force apparatus (SFA) [14–16]. However, these experiments lack a detailed temperature evolution study of a given interface structure. They were performed either at an ambient temperature [13], at some selected temperatures [14], or were exclusively concentrated on nematic or smectic phases [15,16].

In this paper we present experimental results that give direct evidence of structural complexity of real nematic liquid-crystal interfaces. We introduce a new experimental method into this field, the atomic force spectroscopy (AFS). Together with the electric force microscopy introduced recently by Xu *et al.* [17], it represents a new powerful tool on a mesoscopic scale that can give important new information on the structure of liquid-crystal interfaces.

The motivation for this study has been recently renewed interest in the interplay between the nematic and smectic surface-induced order [10,18–20]. This effect significantly increases the structural complexity of the interface and might be relevant in materials with pronounced smectic tendency, such as, for example, in liquid crystals.

We have studied the interface between a silane surfactant covered glass substrate and a 4-cyano-4′-*n*-octylbiphenyl (8CB) nematic liquid crystal in the isotropic phase. The surfactant enforces homeotropic ordering of the liquid crystal at the interface and the formation of smectic layers parallel to

*Author for correspondence. Email address: igor.musevic@ijs.si

the plane of the surface is energetically favored [18]. We have used two different experimental methods to analyze the temperature dependence of the LC structure close to the solid interface: (i) The Brewster angle reflection ellipsometry, which is sensitive to the interfacial nematic ordering of a liquid crystal. The method enabled us to determine an average orientational ordering of the liquid crystal close to the solid surface and as a consequence the coupling energies between the solid surface and the orientational order could be determined. (ii) The atomic force spectroscopy has been used to study the temperature dependence of the structural forces in the isotropic phase, confined between a flat substrate and a small sphere, attached to the atomic force microscope (AFM) cantilever. The method is based on a fact that the free energy of a given thin layer of a liquid crystal between two surfaces depends on the structure of the liquid crystal and consequently on the surface separation. Any change of the separation will therefore cause a force on the confining surfaces, which is measured with piconewton resolution. AFS is sensitive both to the nematic and smectic ordering at the interface.

In our experiments we have observed the following: (i) The ellipsometry experiments on *N*,*N*-dimethyl-*N*-octadecyl-3-aminopropyltrimethoxysilyl chloride (DMOAP) silanated-glass surfaces show complete wetting of these surfaces by the nematic phase of liquid crystals. (ii) The DMOAP surface induces significant smectic ordering of liquid crystals already several degrees above the clearing point, as evidenced from AFS. (iii) The surface smectic amplitude of this presmectic ordering increases when approaching the isotropic-nematic transition from above. (iv) Underneath the pre-smectic ordering there is a well-developed, smecticlike first molecular layer, as observed by AFS. It shows typical smecticlike elasticity and is stable at temperatures far above the clearing point. (v) The first molecular layer is laterally inhomogeneous. It shows irregular voids with a typical lateral dimension of several hundreds of nanometers.

The experimental results have been interpreted within the framework of the phenomenological Landau–de Gennes (LdG) theory. The results agree well with the theory even at the lowest-order expansion of the free energy. We combined the results on the surface nematic coupling obtained from the ellipsometry with the results on the surface smectic order amplitude obtained from force measurements. We were able to determine the coupling energies of liquid-crystal nematic order on homeotropic, DMOAP silanated-glass surfaces, and the coupling energies between the smectic and nematic order.

The experimental methods, procedures, and materials are described in Sec. II. In the theoretical part, Sec. III, the predictions of LdG phenomenological theory, relevant for our study, are derived. The experimental results together with the discussion are presented in Sec. IV, and the conclusions are made in Sec. V. The reflection amplitude ratio, measured in the ellipsometry, is presented for the long-wavelength limit in the Appendix.

II. EXPERIMENTAL

A. Materials

The nematic liquid-crystal 4-cyano-4′-*n*-octylbiphenyl (8CB) has been used in the experiments, as obtained from Merck (Germany). It has the following bulk phase sequence: crystal $\underset{21.5°C}{\leftrightarrow}$ Sm-*A* $\underset{33.5°C}{\leftrightarrow}$ *N* $\underset{40.5°C}{\leftrightarrow}$ *I*.

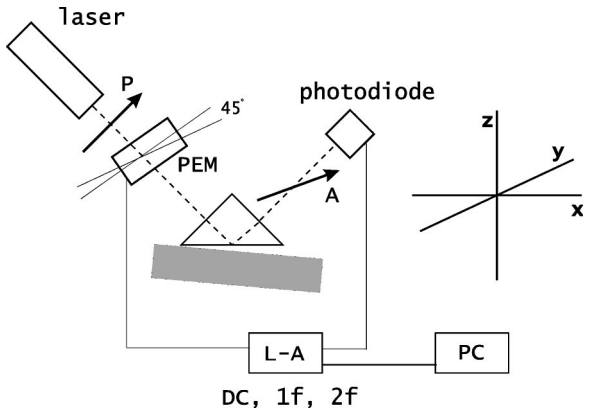

FIG. 1. The schematic of the experimental setup for reflection ellipsometry. The light from the laser source is guided through the polarizer and photoelastic modulator (PEM) with the optical axis at an angle of 45° with respect to the polarizing angle. The light beam is reflected from the lower side of the prism and is detected after passing through the analyzer. dc, first and second harmonics of the modulated light intensity are simultaneously measured, using a lock-in amplifier (L-A) and computer (PC) for data acquisition.

The experiments have been performed on various glass substrates: BK7 glass (Donnelly PD5005/5088) for AFS experiments, BK7 glass and LaSF glass prisms (Edmund Scientific, Zuend Optics) for ellipsometric experiments, and BK7 glass microspheres for force spectroscopy (Polysciences, Inc.). The substrates as well as the glass spheres were cleaned in ultrasonic laboratory detergent bath, rinsed with distilled water, and additionally cleaned with oxygen plasma. After the cleaning procedure, the substrates and the glass spheres, mounted to the AFM cantilevers, have been coated with a monolayer of DMOAP (ABCR), as described elsewhere. A fresh DMOAP solution has been used each time the experiment was performed.

B. Brewster angle reflection ellipsometry

Reflection ellipsometry [21] is known as a very useful method for the determination of the evolution of the orientational surface order in optically anisotropic media [5,6,22,23]. In the reflection ellipsometry, the angular dependence of the polarization of a reflected light is measured. In our experiments, a home-made polarization modulated ellipsometer has been used (Fig. 1). A diode pumped Nd:YVO_4 laser with wavelength $\lambda = 532$ nm, and output power of $P = 100$ mW, has been used as a light source. The light is first guided through the polarizing prism and the PEM which modulates the polarization of light. After that, the beam is reflected from the lower surface of the glass prism, which changes the polarization of the beam. The liquid crystal is filled in the wedge between the glass prism and the glass plate, as schematically presented in Fig. 1. The wedge geometry enabled us to separate the liquid-crystal-surface reflection from the parasite reflections. The reflected beam passes through the analyzer, which is crossed with respect to the

polarizer, and is detected with a photodiode. dc intensity and the first and the second harmonic of the PEM modulated light intensity are simultaneously measured. From this data, the complex ratio r_p/r_s can be determined, where r_s and r_p are the reflection amplitudes of the *s* and *p* polarized light wave, respectively. The amplitude and the phase of the complex ratio are measured separately as $r_p/r_s=\tan\Psi\exp(i\Delta)$. The ratio r_p/r_s contains information about the structure of the interfacial dielectric profile and is most sensitive at the Brewster angle. When the interface is a step function in dielectric profile, the $\tan\Psi$ is 0 at the Brewster angle Θ_B, and the phase Δ jumps for π as the angle of incidence crosses the Brewster angle. As soon as there is some structure of the interface, $\tan\Psi$ is no longer 0 at the Brewster angle, which is now defined as the angle of incidence where $\Delta=\pi/2$. The ellipsometer has been controlled by a personal computer (PC) in such a way that the angle of incidence has been kept very close to the Brewster angle during the linear temperature sweep. By monitoring the reference harmonics, the ellipsometer continuously repeated small angular scans around the Brewster angle and the ellipsometric quantity $\Psi(\Theta_B)=\rho$ has been determined at the Brewster angle. The angular resolution in the Brewster angle was 0.02° and the resolution in Ψ was better than 2×10^{-4}. The results have been interpreted using a model dielectric profile and the long-wavelength approximation was applied, as described in the Appendix.

C. Force measurements

The advantage of AFS force measurements over conventional SFA is, that the experiments can be performed with much smaller samples and the temperature of the sample can be controlled easily with the resolution of 10 mK. The range of forces, applied to the interfaces can be adjusted using different probe diameters and different spring constants of the AFM cantilevers. For large force loads, sharp AFM tips with an apex radius of $\approx$20 nm are usually used, whereas for small force loads, a microsphere of radius $R\approx10$ μm is attached to the AFM cantilever and the force on the microsphere is measured.

A commercial Nanoscope III (Digital Instruments, Santa Barbara, CA) in the force spectroscopy mode has been used for force measurements. In this mode of operation, a time-periodic movement of the surface of the sample is performed in a direction towards the AFM cantilever and the deflection of the cantilever is monitored. The speed of approach is several nm/s and typically 512 force values are collected during approach and retrace cycle. We have equipped the instrument with a double temperature controlled microstage [24] to achieve good temperature stabilization of the order of 10 mK. One heater was integrated in the cantilever holder above the sample and the second independent heater right beneath the sample. The upper heater was formed by a glass plate coated with a transparent indium tin oxide (ITO) layer and was mounted on the cantilever holder just above the cantilever. This glass plate held the drop of liquid crystal, so that the cantilever was always immersed in a liquid crystal. The upper glass plate was heated by controlling the current through the ITO electrode. In this way, the temperature was controlled to better than 10 mK, and the temperature gradient in a liquid crystal were of the order of 1 K/mm. The commercial Si_3N_4 cantilevers (Park Scientific Microlevers) with force constants 0.1 to 0.01 N/m have been used. In some experiments we have used standard tips with an approximate apex radius of 15 nm and in other experiments we have glued a glass sphere of radius $R\approx8$ μm coated with DMOAP onto the cantilever. The resolution of 20 pN has been achieved in force measurements.

III. THEORY

A. Landau–de Gennes description of confined liquid crystal

We have used LdG theory [25] to describe the isotropic-nematic phase transition of a nematic-liquid crystal in the presence of ordering or disordering walls. Within the framework of LdG theory, the free-energy density of a system is expanded in a power series of the order parameters and their derivatives. Because liquid crystal exhibits a narrow nematic phase, which is followed by a Sm-*A* phase, we have to consider both nematic and smectic field contribution to the free energy. The free-energy density is therefore expanded in terms of nematic and smectic-order parameter [19,26].

In practice, the total free-energy density contains a large number of terms and there are no analytical results for the order-parameter interfacial profiles, forces, and ellipticity. As we expect small values of both order parameters in the disordered isotropic phase, only the lowest-order terms are retained and the coupling between both orders is neglected at first. Furthermore, as both surfaces induce homeotropic alignment, the director field is homogeneous and perpendicular to the wall. We set the *z* axis of the coordinate system parallel to the director field and expand the free-energy density in terms of the scalar nematic order parameter $S(z)$, smectic order parameters $\mathbf{\Psi}(z)=\Psi(z)e^{i\Phi(z)}$, and their spatial derivatives. Here, $\Psi(z)$ measures the amplitude of the smectic modulation, $\Phi(z)=(2\pi/a_0)u(z)$ is the phase, related to the layer displacement $u(z)$, and the smectic periodicity is a_0. The bulk free-energy density is

$$f(z)=\frac{1}{2}a_N(T)S^2+\frac{1}{2}L_N\left(\frac{dS}{dz}\right)^2+\frac{1}{2}a_{Sm}(T)\mathbf{\Psi}(z)^*\mathbf{\Psi}(z)+\frac{1}{2}L_{Sm}\frac{\partial\mathbf{\Psi}^*}{\partial z}\frac{\partial\mathbf{\Psi}}{\partial z}. \quad (1)$$

Here $a_N(T)=\alpha_N(T-T_N^*)$ drives the nematic phase transition and $a_{Sm}(T)=\alpha_{Sm}(T-T_{Sm}^*)$ drives the smectic phase transition, where T_N^* and T_{Sm}^* are the temperatures to which isotropic and nematic phase can be undercooled. The coefficients L_N and L_{Sm} of the gradient terms are elastic constants, which describe the increase of the free energy of the system when the order parameters vary in space. Higher-order terms have been neglected, as we analyze the behavior of the system in the vicinity of the phase transition, where higher-order terms are much smaller.

As the free-energy density is decoupled in the two order parameters, both order parameter profiles can be determined by Euler-Lagrange minimization, performed independently

for the nematic and smectic order parameters. Because the resulting interface profiles are different for a semi-infinite sample, relevant for the ellipsometry and a sample sandwiched between two parallel walls, relevant for force measurements, they will be derived separately.

In the ellipsometry only the nematic (orientational) order in the vicinity of a semi-infinite flat surface is visible (see the Appendix). The total free energy of the semi-infinite sample per unit surface area is

$$F_N = \int_0^\infty f(z)dz - GS_0 + W_2 S_0^2, \tag{2}$$

where G and W_2 are the linear and quadratic terms of the energy coupling the orientational order to the surface. The linear term models ordering and the quadratic term models disordering effects of the surface. Following the Euler-Lagrange minimization, the nematic order parameter profile for a semi-infinite sample, where the interface is in the xy plane located at $z=0$, is

$$S(z) = S_0 \exp(-z/\xi_N). \tag{3}$$

Here, S_0 is the value of the nematic order parameter on the surface at $z=0$, and $\xi_N = \sqrt{L_N/a_N}$ is the nematic correlation length. To obtain the value of the order parameter at the surface S_0, the total free energy per unit surface area due to the nematic order F_N has to be minimized with respect to S_0. This minimization yields

$$S_0 = \frac{G}{L_N/\xi_N + 2W_2}. \tag{4}$$

The complete nematic profile therefore combines Eqs. (3) and (4). The ellipsometric ratio at a Brewster angle can be calculated using Eqs. (3) and (4) and expressed in a closed form, as shown in the Appendix.

B. Mean-field nematic and smectic forces

In the force measurements both orientational nematic and positional smectic orders contribute to the force between a sphere and a surface. The geometry is in this case different, as we have one curved surface of a sphere and a flat surface of the substrate. The easiest way to calculate the force on a sphere in the vicinity of a flat surface, is by applying the Derjaugin approximation [1]. It relates the force between the sphere and flat surface separated by a distance d, to the interaction free energy per unit surface area between two parallel and infinite flat surfaces separated by d,

$$\mathcal{F}(d) = 2\pi R F_{int}(d). \tag{5}$$

Here, $\mathcal{F}$ is the force on a sphere, R is the radius of the sphere, and $F_{int}(d) = F(d) - F(\infty)$ is the interaction free energy per unit surface area, where $F(d) = \int_{-d/2}^{d/2} f(z)dz + W_{surf}$. W_{surf} is the surface energy contribution. In order to account only for the interaction part of the free energy, relevant for the force, the reference bulk configuration free energy has been subtracted. Note that surface contributions are doubled with respect to the semi-infinite sample, where only one surface is present.

The use of the Derjaugin approximation can be justified, if the range of the interaction and the distance between the sphere and the surface d are much less than the radius of the sphere R. This is true in our case, where the correlation lengths that measure the range of interaction are of the order of 10 nm and a typical radius of the sphere is a thousand times larger, $R = 10\ \mu$m.

The interaction free energy per unit surface area of the LC sample confined between two parallel plates is in our case a sum of decoupled smectic and nematic contribution, $F_{int}(d) = F_{int\ Sm}(d) + F_{int\ N}(d)$. The nematic part of the interaction energy can easily be obtained following de Gennes calculation for presmectic forces [27]. The nematic part of the free energy per unit surface area is

$$F_N(d) = \frac{1}{2} L \left[S \frac{dS}{dz} \right]_{-d/2}^{d/2} - 2GS_0 + 2W_2 S_0^2. \tag{6}$$

The profile for the nematic order parameter is in this case symmetric as obtained by solving Euler-Lagrange equations with symmetric boundary conditions

$$S(z) = S_0(d) \cosh\frac{z}{\xi_N} \Big/ \cosh\frac{d}{2\xi_N}. \tag{7}$$

$S_0(d)$, the nematic order parameter value on the surface can be again obtained by the minimization of the total free energy per unit surface area given by Eq. (6). It depends on the wall separation and surface coupling energies:

$$S_0(d) = \frac{G}{2W_2 + L_N/\xi_N \tanh\dfrac{d}{2\xi_N}}. \tag{8}$$

The interaction mean-field nematic free energy is

$$F_{int\ N}(d) = \frac{G^2}{2W_2} \left[\frac{1}{1 + 2\xi_N W_2 \coth(d/2\xi_N)/L_N} - \frac{1}{1 + 2\xi_N W_2/L_N} \right], \tag{9}$$

which results in an attractive mean-field nematic force.

For the mean-field smectic force we follow the derivation performed by Ziherl [20] and previously done by de Gennes [27] and Richeti [16]. We assume fixed amplitude of the smectic order on the surfaces $\Psi(\pm d/2) = \Psi_0$ and fixed position of the first smectic layer next to the wall (phase) $\Phi(\pm d/2) = \pm \Phi_0/2$. Here, $\Phi_0 = 2\pi(d/a_0 \mod 1)$ is the phase mismatch related to the compression or dilation of the smectic layers, whose thickness d is not an integer multiple of the unperturbed smectic period a_0. The resulting mean-field smectic interaction free energy [16,20] is

$$F_{int\ Sm}(d)=\frac{L_{Sm}\Psi_0}{\xi_\parallel}\left[\coth\frac{d}{\xi_\parallel}-\frac{\cos[2\pi(d-d_0)/a_0]}{\sinh(d/\xi_\parallel)}-1\right]. \tag{10}$$

Here $\xi_\parallel=\sqrt{L_{Sm}/a_{Sm}}$ is the smectic correlation length in the direction along the smectic normal and d_0 is the phase offset, which is due to the uncertainty of the determination of zero surface separation in the AFM force measurements.

So far we have neglected any nematic-smectic coupling terms in the Landau–de Gennes free-energy expansion. Here we consider a simple model, which introduces the lowest-order coupling term in free-energy density expansion. By symmetry, the lowest-order coupling term is $f_{N\ Sm}=\Gamma S|\Psi|^2$ [26]. Here, Γ is the coupling energy, which is negative if both nematic and smectic fields enhance each other. We assume that in the first-order approximation the pretransitional nematic order only amplifies the smectic order parameter amplitude on the surface and that the coupling is so weak, that it does not change the nematic order significantly. We also assume that the coupling has practically no effect on the order-parameter profiles that were calculated in the absence of the coupling.

We therefore only consider the increase of the smectic order parameter at the surface of a semi-infinite sample due to the coupling to the nematic order parameter. In this case the smectic free-energy density is

$$F_{Sm}=\int_0^\infty\left[\frac{1}{2}a_{Sm}\Psi^2+\frac{1}{2}L_{Sm}\left(\frac{d\Psi}{dz}\right)^2+\Gamma\Psi^2S\right]dz + w_{Sm}(\Psi_0-\Psi_a)^2, \tag{11}$$

where Ψ_a is the smectic order parameter amplitude preferred by the surface and w_{Sm} is the smectic coupling energy of the surface. For $S(z)$ we take the unperturbed profile from Eq. (3) and we take $\Psi(z)=\Psi_0\exp(-z/\xi_\parallel)$ for the smectic order parameter amplitude profile, where $\xi_\parallel$ is the smectic correlation length. Minimization of the total free energy per unit surface area with respect to Ψ_0, yields

$$\Psi_0=\Psi_a\Big/\left(1+\frac{L_{Sm}}{2w_{Sm}\xi_\parallel}+\frac{\Gamma\xi_{Sm}\xi_N S_0}{w_{Sm}(\xi_\parallel+2\xi_N)}\right). \tag{12}$$

Here S_0 is that given by Eq. (4). One can see, that the smectic order at the surface Ψ_0 is enhanced either (i) via the smectic surface coupling energy (i.e., the second term in the denominator), which is expected to be temperature independent, or, (ii) via the nematic-smectic coupling, given by the third term in the denominator. This coupling term induces temperature dependence of the surface smectic amplitude in the vicinity of the isotropic-nematic phase transition, because the nematic correlation length changes significantly in this region.

C. Van der Waals force between surfaces immersed in a liquid crystal

Van der Waals dispersion forces between surfaces are present in all cases where the dielectric properties of the interacting media are different from the dielectric properties of the media across which they interact. For a nonretarded van der Waals interaction, the force between a sphere and a flat surface is $\mathcal{F}_{VdW}=-AR/6d^2$ [1], where d is the separation between the sphere and the surface, R is the radius of the sphere, and A is the Hamaker constant for the interaction between the media of the sphere and the media of the flat surface across the media between both surfaces. We have calculated the Hamaker constants for the interaction across the liquid crystal using the Lifshitz theory described in [1]. For the calculation of the Hamaker constant, one needs to know the static and the optic dielectric constants of all three media. Furthermore, as the liquid crystal in the bulk isotropic phase is an anisotropic and spatially inhomogeneous media close to the surfaces, because of the surface-induced order, we have used the arithmetic mean of the parallel and perpendicular part of dielectric constants, as well as the spatial average of the dielectric constant profile. In Table I, Hamaker constants are given for the interaction between two BK7 glass surfaces and a BK7 or LaSF glass surface across the liquid crystal.

TABLE I. Hamaker constants A calculated from the Lifshitz theory for the interaction between two identical BK7 glass surfaces and BK7-LaSF glass surfaces across isotropic liquid crystal.

Interaction media	A
BK7 glass-liquid-crystal-BK7 glass	8.4×10^{-22} J
LaSF glass-liquid-crystal-BK7 glass	-1.6×10^{-21} J

IV. RESULTS

In this section we separately present the results obtained from ellipsometry, where the coupling energies of the nematic order with surface for liquid crystal have been determined. Then we discuss the smectic order observed by AFM force measurements and the observability of other force contributions in force experiments.

A. Ellipsometry

Using Brewster angle reflection ellipsometry, we have measured the temperature dependence of the complex ellipsometric ratio r_p/r_s, when cooling down liquid crystal from the isotropic into the nematic phase. The measurements have been performed as described in Sec. II B and LaSF and BK7 glass prisms have been used as substrates. The nematic correlation length, which measures the depth of the interface, is much smaller than the wavelength of light, so the long-wavelength limit expansion of the ellipsometric ratio can be applied as described in the Appendix. Figure 2 shows the measured temperature dependence of the ellipsometric invariant $\mathcal{I}_1$ for liquid crystal (open circles) on DMOAP coated LaSF and BK7 surfaces. The ellipsometric invariant $\mathcal{I}_1$ is in the first-order approximation to Drude's expression [28] proportional to the adsorption parameter Γ, used by other authors [5,6]. The solid lines are the best-fit ellipsometric invariants $\mathcal{I}_1$ for liquid crystal, calculated from the Eq. (A1). Linear and quadratic coupling energies between the nematic order

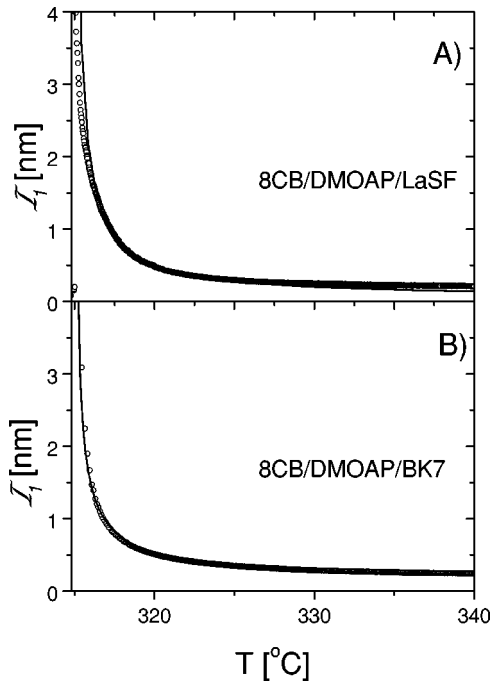

FIG. 2. The temperature dependence of the ellipsometric invariant $\mathcal{I}_1$ for the isotropic phase of liquid crystal [see Eq. (A4)], as measured by the Brewster angle ellipsometry. (A) Isotropic liquid crystal on LaSF glass substrate coated with a monolayer of DMOAP. (B) Isotropic phase of liquid crystal on the DMOAP coated BK7 glass. Open circles represent the ellipsometry invariant, as calculated from the measured ellipsometric ratio at the Brewster angle. The full lines are the best fit to Eq. (A4), with surface couplings given in Table II.

parameter and the surface were determined from the fitting procedure following Eq. (A4) and S_0, given by Eq. (4). They are listed in Table II.

We should comment on this analysis by noting that we have taken here a different approach as, for example, Chen *et al.* [5]. Whereas they have used a better approximation of the nematic order parameter profile (to the fourth order of LdG expansion), derived by Tarczon [29], we have sacrificed here some precision in the profile (which also introduces additional two barely known parameters), but have made no simplifications in the integration of the Eq. (A4). We have checked that the second-order correction to the first-order expansion of Eq. (A4), can be as high as 20%. This is more than the correction due to a slightly perturbed order-parameter profile, resulting from the harmonic approximation of a LdG free-energy expansion. Furthermore, we have separately remeasured the parameter a_N for liquid crystal,

TABLE II. The surface coupling ordering (G) and disordering (W_2) energies for liquid crystal on DMOAP coated LaSF and BK7 glass, determined from the Brewster angle ellipsometry.

Substrate	G	W_2
BK7	1.4×10^{-4} J/m^2	5.6×10^{-5} J/m^2
LaSF	1.5×10^{-4} J/m^2	6.0×10^{-5} J/m^2

using dynamic light scattering in the vicinity of the isotropic-nematic phase transition. The slowing down of the order-parameter relaxation rate in the bulk sample of liquid crystal was measured as a function of temperature, as described elsewhere [30]. This gave us $a_N = 1.6\times10^5$ J/K m^3 for liquid crystal, where the viscosity has been taken from Coles [31]. The elastic constant L_N was determined to be 3×10^{-12} N by iterative fitting of the ellipsometry data. The values of the surface coupling energies were determined by fitting of the ellipsometric data and are given in Table II. One can see that the nematic ordering term (G) is in both cases dominant over the disordering term (W_2).

The surface coupling energies are comparable in magnitude to the values given by other authors.

Note that the wetting of the nematic phase on DMOAP covered surfaces is complete, the surface order parameter S_0 exceeds the bulk nematic order parameter, and the ellipsometric ratio diverges at the phase transition as previously also reported by Chen [5].

B. Surface force measurements

Two different sets of AFM force experiments have been performed at the liquid-crystal–silanated-glass interface. First we have probed this interface with a sharp, commercial Si_3N_4 AFM tip with a typical apex radius of 15–20 nm. In these experiments rather large force loads have been applied to the surface and we could study elastic properties of the very first molecular layer. In a second set of experiments, we have measured interfacial forces between a DMOAP covered flat glass surface and a glass sphere of radius $R\approx10$ μm. This gave us much lower force loads, but also increased force sensitivity.

1. Observation of a surface adsorbed first molecular layer

A typical force vs separation plot, as observed in the force measurements using a sharp AFM tip is shown in Fig. 3. At a distance of approximately 4 nm there is some small attractive force, which causes a tip instability. Here, the tip is unstable if the gradient of the attractive force is larger than the force constant of the cantilever, and is suddenly attracted towards the surface. This attraction stops at a distance around 3.3 nm from the surface, where the force changes to repulsion. The force is increasingly repulsive until the distance of separation of ≈1.3 nm, where there is a sudden jump of the tip into the contact with the glass surface. We interpret this observation as follows. After the first attraction, which is most probably due to the liquid-crystal structure at the surface, the tip touches the first layer of liquid-crystal molecules, which are strongly adsorbed onto the surface. The thickness of this first molecular layer is always of the order of molecular length and also increases with increasing molecular length. After applying an additional force on the tip via the elastic cantilever, the molecular layer is compressed and elastically deformed. Finally, when the force load is high enough, the surface-adsorbed layer ruptures and the tip comes into hard contact with the rigid substrate. Here, there is practically no observable additional indentation as the force load is further increased. We have performed force

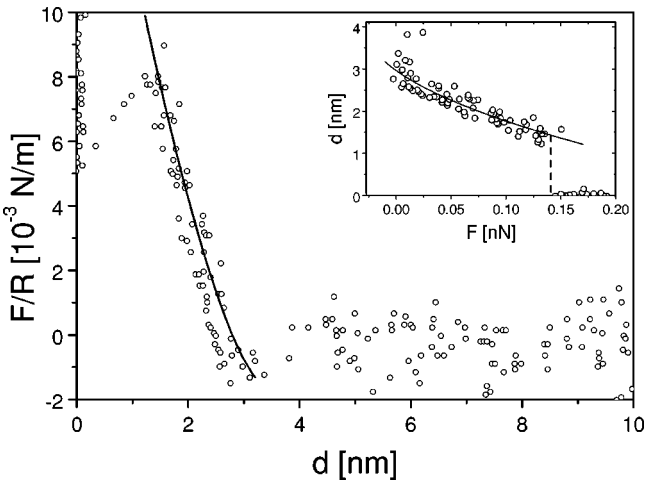

FIG. 3. A typical force plot, observed with a sharp AFM tip immersed in the isotropic phase of liquid crystal, when approaching and indenting a LaSF glass surface coated with DMOAP. The data were measured at $T-T_{NI}=8$ K. The solid lines are fits to the Hertz model and give the equilibrium thickness of the first molecular layer of 3.2 (1 ± 0.06) nm and the elastic modulus of the layer $E^*=1.2\times10^7$ (1 ± 0.3) N/m^2. The inset shows the same data, where the thickness of the first molecular layer is shown vs applied force.

scans, where we have stopped applying the force before the layer had raptured. We have clearly observed that in this case there was no hysteresis in indentation between increasing and decreasing force scans. We therefore conclude that the compression of the surface layer is purely elastic. We have also made sure that this layer cannot be attributed only to the silane monolayer, by performing the same experiment using hexane instead of liquid crystal. At the hexane-DMOAP interface we have observed repulsive, exponentially decaying force. The decaying length was typically ≈2.5 nm and we could not observe any rupturing of the silane-hexane layer. This clearly indicates that (i) silane molecules are strongly position-ally anchored to the glass and contribute a small polymer-entropiclike repulsive force, and (ii) the rupturing is definitely attributed to the surface-adsorbed layer of liquid-crystalline molecules.

We have followed the temperature stability of this layer deep into the isotropic phase. The layer could be observed even 20 K above the T_{NI}, with no observable change of the elastic modulus in this temperature interval. This indicates that the first layer of liquid-crystalline molecules is very strongly coupled to the substrate.

We have analyzed the elastic deformation of the first molecular layer within two continuum elastic models: (i) the Hertz indentation model, and (ii) the elastic foundation model [32]. In the popular Hertz model of indentation, the elastic deformation of a semi-infinite elastic sample with a rigid sphere is considered. The depth of indentation is $\delta=\sqrt[3]{[}39\mathcal{F}^2/16RE^{*2}$, where $\mathcal{F}$ is the force applied to the spherical tip, R is the radius of the sphere, and $E^*=E/(1-\nu^2)$, where E is the Young's elastic modulus and ν is the Poisson's number. The elastic modulus of the first molecular layer, obtained from the fit to Hertz's model, is in all cases of the order 10^7 (1 ± 0.3) N/m^2, which is typical for a smectic liquid crystal [33].

The problem of applying the Hertz model of indentation to our experiment could be due to the fact that the AFM tip indents a relatively thin elastic layer on a semi-infinite hard substrate. In this case the elastic ''foundation layer'' model should be more appropriate. In this model an elastic layer of thickness h on the rigid base is considered. This layer is described as a ''mattress,'' which is made of uncoupled elastic stabs springs, of an elastic modulus K. Following Johnson [32], the depth of indentation by a sphere of radius R is $\delta=\sqrt{h/\pi RK}\sqrt{F}$. By fitting the experimental data for compression of the first molecular layer we obtain $K=2.3\times10^6$ (1 ± 0.1) N/m^2 and the thickness of the layer is 3.75 (1 ± 0.05) nm. According to Johnson, E^* and K are connected by $E^*=Kr/1.7h$, where r is the radius of the contact. The fit to elastic mattress model gives us $E^*\approx3.5\times10^6$ N/m^2, which is of the same order as the elastic modulus, obtained from Hertz's model. The continuum approach of these models to the analysis of elastic indentation of a thin adsorbed layer is justified, if the fluctuation contribution to the compressibility is small. Since the layer elastic properties are temperature independent, we conclude that it is strongly anchored to the surface and thermal fluctuations must be suppressed. We therefore conclude that the constitution of the first molecular layer adsorbed to the surface is similar to smectic. The same was observed on similar experiments performed on nematic liquid crystals 5CB and MBBA, which also show the presence of the first molecular layer with similar properties. The thickness of the layer scales with the length of fully extended liquid crystalline molecule, was presented in our previous article [34].

We have also studied the lateral coverage of the silanated-glass surface with first molecular layer. During the experiments, we have observed, that the characteristic ''steplike'' force plot, indicating the first molecular layer, was present in some cases and absent in other. We have therefore performed a very large number of force plot experiments on different samples and on different places. The type of force plots with rupturing step, that indicates the presence of the layer, can be observed on approximately 70% of the surface. In other cases there is no step and no smecticlike first molecular layer. We have concluded that the first molecular layer appears in a form of clusters or a layer with voids. These smectic clusters are difficult to observe directly by imaging, since the force of the tip on the sample during imaging is so large that it seriously damages the layer [35].

In Fig. 4 we present an indirect image of the surface coverage by the first molecular layer. This image was taken by performing a large number of force measurements in a predetermined, regular array of points across a surface area of 10×5 μm. The presence of the first, smecticlike molecular layer is indicated by a white region, whereas ''voids'' (i.e., the absence of) indicate that there is no smecticlike first molecular layer.

The lateral dimension of voids can only be estimated from these measurements and is in the range 10 nm$<R_c<100$ nm. It is not clear, if this type of coverage is intrinsic to this interface because of the type of growth, or just reflects the inhomogeneities of the glass substrate underneath.

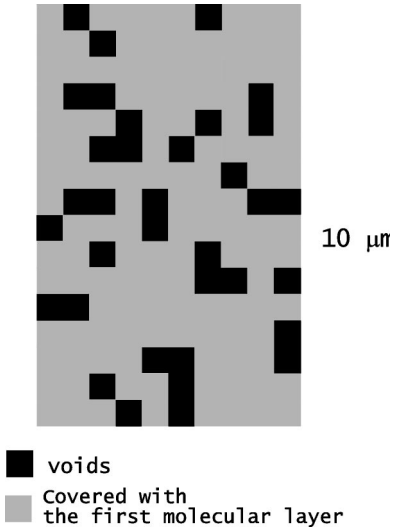

FIG. 4. The coverage of the silanated-glass surface with smecticlike surface layer, as determined from the force measurements. White squares indicate that a typical step in the force-distance curve was detected at that position. Dark squares indicate points with no step and, therefore, no smectic coverage.

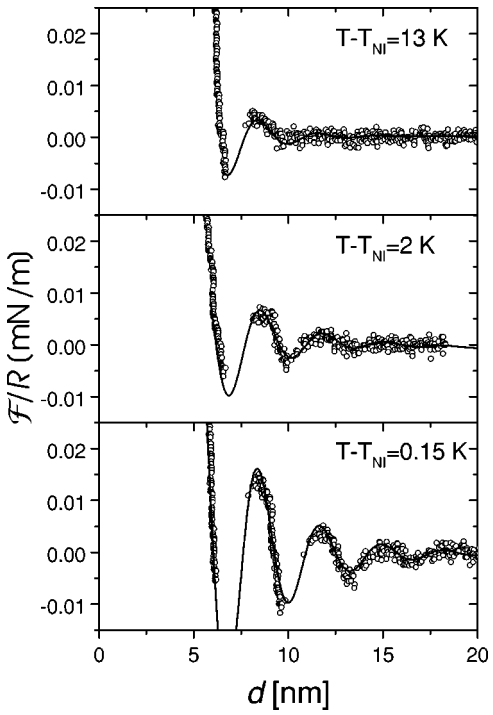

FIG. 5. Normalized structural force as a function of separation between a 8.5 μm silanated-glass sphere and a silanated-BK7-glass substrate in the bulk isotropic phase. The solid line is a fit to the sum of van der Waals, mean-field smectic, and mean-field nematic force, described in the text.

2. Observation of presmectic ordering at a nematic-solid interface

Interfacial mean-field nematic and smectic forces due to the liquid-crystal structure close to the interface are very weak and the sensitivity of the AFM using a sharp AFM tip is too low to detect them. These forces can, however, be dramatically increased by increasing the radius of curvature R of the curved surface. For this reason we have attached a glass microsphere to the commercial AFM cantilever and coated it with DMOAP. Using this sphere-flat surface geometry, the interfacial forces are increased by a factor of 1000 and we have detected in all experiments on 8CB liquid crystal typical oscillatory force curves, shown in Fig. 5. These force profiles can be attributed to the presmectic force in the isotropic phase, arising from the surface-induced smectic order.

The force profiles have been analyzed by considering all relevant forces that are expected to contribute significantly: (i) van der Waals force with Hamaker constant calculated as described in Sec. III C, (ii) attractive nematic mean-field force given by Eq. (9), with surface coupling constants as determined in the ellipsometry experiments, (iii) oscillatory presmectic force given by Eq. (10). The analysis of the separation dependence of these forces has clearly shown that the zero of separation (which cannot be determined unambiguously from the AFM data) has to be chosen with an offset of 6 nm. This fact can easily be explained by taking into account our previous measurements made with a sharp AFM tip. The normalized force load $\mathcal{F}/R$, which is necessary to rupture the first molecular layer of thickness 3.4 nm, is two orders of magnitude larger than the corresponding values available in the experiments with attached sphere. We conclude that in the experiments with attached sphere, the glass surfaces cannot be brought closer than $\approx$6 nm, which equals the thickness of two surface adsorbed molecular layers, one on each surface.

Solid lines in Fig. 5 represent the best fit to the sum of the mean-field smectic structural force, mean-field nematic and van der Waals force for a BK7-8CB-BK7 interface. The nematic mean field and van der Waals forces are here of quite small magnitude, and become more important for smaller separations. The fit is excellent and allows us to determine the surface-induced smectic order and smectic correlation length.

Figure 6 shows a similar analysis for the structural forces at the LaSF-8CB-BK7 interface. We have included force plots from both types of experiments on the same graph. It is interesting to note that the experiment indeed detects a repulsive van der Waals force. It is due to the fact, that the index of refraction of liquid crystal is in between the index of refraction of BK7 and LaSF glass.

The modeling structural force is in all experiments in remarkable agreement with experimental results on both substrates and it allows a determination of (i) the smectic order parameter Ψ_S on the surface, (ii) smectic correlation length $\xi_\parallel$, and (iii) smectic periodicity a_0. By taking $L_{Sm}=5$ pN [20], we obtain from data on Fig. 6, the smectic amplitude on the surface $\Psi_S=0.15$ (1 ± 0.15), smectic correlation length $\xi_\parallel=3.2$ (1 ± 0.15) nm, and smectic periodicity $a_0=3.2$ (1 ± 0.02) nm. The smectic periodicity is in excellent agreement with reported bulk values [36] and indicates bilayer presmectic ordering at the surfaces. We should again note that in contrast to our previous study [34], a different zero of separation has been chosen. This is more consistent in view of the presence of the first bilayer, adsorbed on both

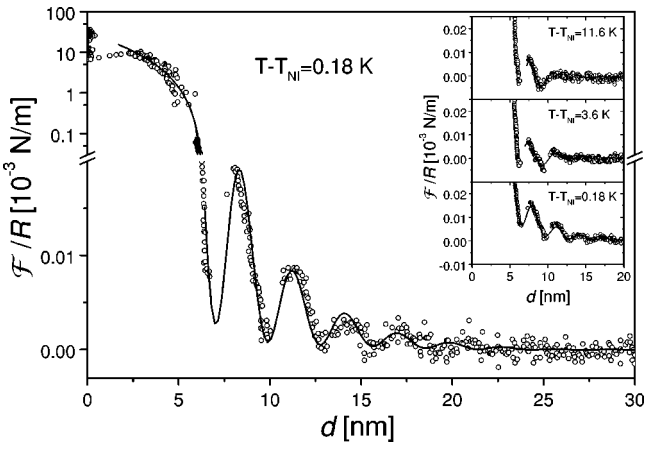

FIG. 6. Normalized structural force as a function of the separation between a 10 μm silanated-BK7-glass sphere and a silanated-LaSF-glass substrate in the bulk isotropic phase at $T-T_{NI}=0.18$ K. The experiments performed with a sharp tip and with an attached glass sphere are plotted together on the same graph. The upper-half of the graph has a logarithmic scale in order to represent both measurements together. The solid line in the lower part of the graph is a fit to the sum of van der Waals, mean-field nematic, and presmectic force. The solid line on the upper-half of the graph is a fit to the mattress model of squeezing the elastic layer with a thickness of 6.5 nm. The inset shows a series of force plots on the same system at different temperatures. Solid lines are fits to the model described in the text.

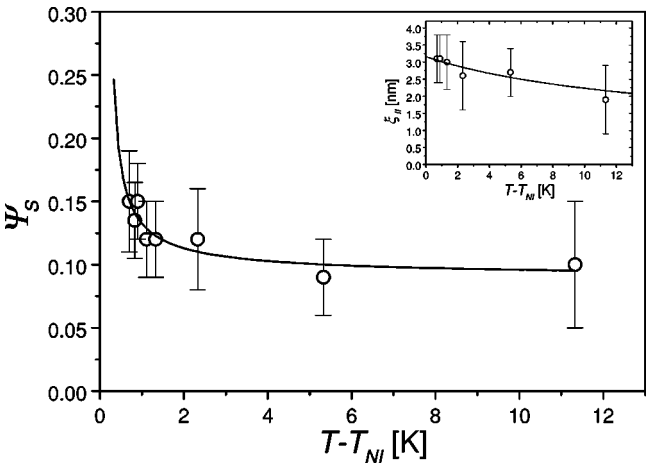

FIG. 7. Temperature dependence of the surface smectic amplitude Ψ_S, calculated from the AFM experimental data. The solid line is an expected amplitude of the smectic order parameter on the surface due to the coupling with the nematic order parameter. The inset shows the temperature dependence of smectic correlation length as determined from the AFM experiments. The solid line represents x-ray measurements of Davidov *et al.* [36].

surfaces. It also explains, why the detected force contributions due to the nematic ordering and van der Waals force are very small.

In our previous report we have pointed out that the smectic ordering of the first bilayer can be estimated from the force, which is needed to rupture this layer with a tip. Since we know the forces, which are needed to rupture the presmectic layers with a sphere, we can linearly interpolate the dependence of the rupturing force on the smectic order-parameter amplitude. This leads to an estimate that the smectic amplitude of the first layer is $\Psi_S \approx 0.3$, and also agrees well with surface smectic amplitudes, obtained from the fits shown in Figs. 5 and 6, obtained with a choice of zero with a separation offset of 6 nm.

Figure 7 shows the temperature dependence of the smectic amplitude on the surface Ψ_S and the smectic correlation length $\xi_\parallel$ for the system BK7-8CB-BK7. The smectic order-parameter amplitude increases close to the bulk nematic to the isotropic phase transition. We conclude that this increase is driven by the coupling between the smectic and nematic order parameters, which increases near the phase transition. We apply the first-order coupling approximation with parameters $L_N=2$ pN and $L_\parallel=5$ pN, for the smectic correlation length $\xi_\parallel=3.1$ nm and for bare nematic correlation length $\xi_N=5.5$ nm. We assume that the preferred surface smectic amplitude is $\Psi_a=0.7$, which does not have significant influence on the overall analysis of the surface coupling energies. The calculated value for the smectic coupling with the surface is $w_{Sm} \approx 2\times 10^{-4}$ J/m^2 and the value of the smectic-nematic coupling energy is $\Gamma = 1.7\times 10^6 (1\pm 0.1)$ J/m^3. This result is in agreement with the value calculated from the jump in the nematic order parameter at the first-order nematic-smectic phase transition for liquid crystals [37].

V. CONCLUSION

In this paper we have presented an experimental analysis of the interface between a nematic liquid crystal in the isotropic phase and a solid substrate which induces homeotropic ordering of a liquid crystal. We have applied two complementary experimental techniques and we have analyzed the results within a simple LdG theory of surface-induced ordering. We have observed that the interface is quite complex already in the isotropic phase of a liquid crystal. The first molecular layer that is strongly adsorbed to the surface, is smecticlike and incompletely covers the surface. A large pressure has to be applied in order to rupture this layer, which indicates that LC molecules are also to some extent laterally anchored to the surface. This could be explained by the penetration of LC molecules between the chemically adsorbed silane molecules [15]. This layer is followed by a combination of a prenematic and a presmectic ordering of liquid crystals that is nicely described with LdG theory. The two order parameters are clearly coupled, as evidenced from the pretransitional increase of the smectic ordering, which is due to a strong increase of the nematic order. The LdG analysis shows that the results of the ellipsometry and AFM experiments can be consistently described using a single set of surface coupling and structural parameters. Moreover, we have shown that force spectroscopy experiments give access to many new liquid-crystalline interfacial parameters, not easily obtained by other methods. For example, smectic amplitude at a surface as well as smectic correlation length can routinely be obtained, which gives new possibilities for the investigations of liquid-crystal interfaces.

APPENDIX: ELLIPSOMETRY

Reflection amplitudes ratio measured with ellipsometry carries information on the structure and thickness of the surface layer, where dielectric properties vary. Generally the results are difficult to interpret, but if the thickness of the interface is small compared to the wavelength of light, the long-wavelength limit expansion can be applied. In the case of surface orientational order, the thickness of the interface is related to the nematic correlation length. Long-wavelength limit can be applied when $\lambda \gg \xi_N$, where λ is the wavelength of the reflected light and ξ_N is the nematic correlation length. At the Brewster angle the ellipsometric ratio r_p/r_s can be written to the first order in interfacial thickness for a thin, optically anisotropic film [28]

$$\left(\frac{r_p}{r_s}\right)_{\Theta_B} = \frac{\pi}{\lambda}\frac{\sqrt{\epsilon_1+\bar{\epsilon}}}{\epsilon_1-\bar{\epsilon}}\mathcal{I}_1, \tag{A1}$$

where ϵ_1 and $\bar{\epsilon}$ are the optical dielectric constant of the glass (medium where the light comes from) and the isotropic liquid crystal, respectively, and the invariant $\mathcal{I}_1$ is

$$\mathcal{I}_1 = \int_0^\infty \left(\epsilon_1 + \bar{\epsilon} - \frac{\epsilon_1\bar{\epsilon}}{\epsilon_z(z)} - \epsilon_x(z)\right) dz, \tag{A2}$$

where ϵ_z and ϵ_x are the optical dielectric constants in the directions perpendicular and parallel to the surface. The anisotropy in the dielectric constant is a measure of the nematic order parameter [37]:

$$\epsilon_x(z) = \bar{\epsilon} + \frac{1}{3}\Delta\epsilon S(z),$$

$$\epsilon_z(z) = \bar{\epsilon} - \frac{2}{3}\Delta\epsilon S(z), \tag{A3}$$

where $\Delta\epsilon$ is the maximal anisotropy at $S=1$. The invariant $\mathcal{I}_1$ for a nematic profile given in Eq. (3) can be calculated by integrating Eq. (A2) with Eqs. (A3). The result is

$$\mathcal{I}_1 = \xi_N\left[\epsilon_1 \ln\left(1 - \frac{2\Delta\epsilon S_0}{3\bar{\epsilon}}\right) - \frac{1}{3}\Delta\epsilon S_0\right], \tag{A4}$$

where S_0 is given by Eq. (4).

[1] J. Israelachvily, *Intermolecular and Surface Forces* (Academic, New York, 1992).
[2] P. Sheng, Phys. Rev. Lett. **37**, 1059 (1976).
[3] K. Miyano, Phys. Rev. Lett. **43**, 51 (1979).
[4] J. P. Nicholson, J. Phys. (France) **49**, 2111 (1988).
[5] W. Chen, L. J. Martinez-Miranda, H. Hsiung, and Y. R. Shen, Phys. Rev. Lett. **62**, 1860 (1989).
[6] H. Hsiung, T. Rasing, and Y. R. Shen, Phys. Rev. Lett. **57**, 3065 (1986).
[7] P. Guyot-Sionnest, H. Hsiung, and Y. R. Shen, Phys. Rev. Lett. **57**, 2963 (1986).
[8] G. P. Crawford, D. K. Yang, S. Žumer, D. Finotello, and J. W. Doane, Phys. Rev. Lett. **66**, 723 (1991).
[9] G. P. Crawford, R. J. Ondris-Crawford, J. W. Doane, and S. Žumer, Phys. Rev. E **53**, 3647 (1996).
[10] P. Ziherl, M. Vilfan, N. Vrbančič-Kopač, S. Žumer, R. J. Ondris-Crawford, and G. P. Crawford, Phys. Rev. E **61**, 2792 (2000).
[11] B. M. Ocko, Phys. Rev. Lett. **64**, 2160 (1990).
[12] G. S. Iannacchione, J. T. Mang, S. Kumar, and D. Finotello, Phys. Rev. Lett. **73**, 2708 (1994).
[13] J. S. Foster and J. E. Frommer, Nature (London) **333**, 542 (1988).
[14] R. G. Horn, J. N. Israelachvili, and E. Perez, J. Phys. (France) **42**, 39 (1981).
[15] M. Ruths, S. Steinberg, and J. N. Israelachvili, Langmuir **12**, 6637 (1996).
[16] P. Richetti, L. Moreau, P. Barois, and P. Kekicheff, Phys. Rev. E **54**, 1749 (1996).
[17] L. Xu, M. Salmeron, and S. Bardon, Phys. Rev. Lett. **84**, 1519 (2000).
[18] T. Miyazaki, H. Hayashi, and M. Yamashita, Mol. Cryst. Liq. Cryst. **330**, 367 (1999).
[19] A. Poniewierski and A. Samborski, Phys. Rev. E **51**, 4574 (1995).
[20] P. Ziherl, Phys. Rev. E **61**, 4636 (2000).
[21] R. M. A. Azzam and N. M. Bashara, *Ellipsometry and Polarized Light* (North-Holland, Amsterdam, 1977).
[22] R. Lucht and C. Bahr, Phys. Rev. Lett. **78**, 3487 (1997).
[23] P. D. Schrijver, C. Glorieux, W. V. Dael, and J. Thoen, Liq. Cryst. **23**, 709 (1997).
[24] I. Muševič, G. Slak, and R. Blinc, Rev. Sci. Instrum. **67**, 2554 (1996).
[25] P. G. de Gennes, *The Physics of Liquid Crystals* (Clarendon, Oxford, 1974).
[26] I. Lelidis and G. Durand, Phys. Rev. Lett. **73**, 672 (1994).
[27] P. G. de Gennes, Langmuir **6**, 1448 (1990).
[28] J. Lekner, *Theory of Reflection* (Martinus Nijhoff, Dordrecht, 1987).
[29] J. C. Tarczon, J. Chem. Phys. **73**, 1994 (1980).
[30] R. Blinc and I. Muševič, *Handbook of Liquid Crystals* (Wiley-VCH, Weinheim, 1998), Vol. 2 A, Chap. III.
[31] H. J. Coles, Mol. Cryst. Liq. Cryst. **49**, 67 (1978).
[32] K. L. Johnson, *Contact Mechanics* (Cambridge University Press, New York, 1985).
[33] J. Yamamoto and K. Okano, Jpn. J. Appl. Phys. **30**, 754 (1991).
[34] K. Kočevar, R. Blinc, and I. Muševič, Phys. Rev. E **62**, R3055 (2000).
[35] K. Kočevar and I. Muševič, Liq. Cryst. **28**, 599 (2001).
[36] D. Davidov, C. R. Safinya, M. Kaplan, S. S. Dana, R. Shaetzing, R. J. Birgenau, and J. D. Lister, Phys. Rev. B **19**, 1657 (1979).
[37] R. G. Horn, J. Phys. (Paris) **38**, 105 (1978).